

Hyperspherical elliptic coordinates treatment of muon transfer from muonic hydrogen to atomic oxygen

Arnaud Dupays, Bruno Lepetit, J. Alberto Beswick, and Carlo Rizzo
*Laboratoire Collisions, Agrégats, Ractivité, IRSAMC,
Université P. Sabatier, 31062 Toulouse, France*

Dimitar Bakalov
INRNE, Bulgarian Academy of Sciences, Sofia, Bulgaria

Quantum-mechanical calculations of muon transfer between muonic hydrogen and an oxygen nuclei for s waves and collision energies in the range $10^{-3} - 10^3$ eV, are presented. Close-coupling time-independent Schrödinger equations, written in terms of hyperspherical elliptic coordinates were integrated along the hyper-radius to obtain the partial and total muon-transfer probabilities. The results show the expected Wigner-Bethe threshold behavior up to collision energies of the order of 10^{-2} eV and pronounced maxima at 10^2 eV which can be interpreted in terms of crossings between potential energy curves corresponding to the entrance channel state $(p\mu)_{1s} + O$ and two product channels which asymptotically correlate to $p + (O\mu)_{n=5,6}$. The population of the final states with different orbital angular momenta is found to be essentially independent of energy in the range considered in this work. This can be attributed to a strong selection rule for the conservation of the quantum number associated to one of the elliptic hyperangles.

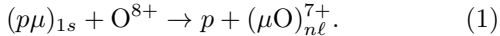
PACS numbers: 36.10.Dr

Keywords:

I. INTRODUCTION

Negative muon transfer between muonic atoms (muonic hydrogen, for instance) and other atoms or molecules has been extensively studied in the framework of muon catalyzed nuclear fusion (see Ref. [1] and literature cited therein). Also, the structural and spectroscopic properties of these species are of interest for metrology and in tests of quantum electrodynamics [2, 3].

Recently, several theoretical [2, 4, 5, 6, 7] and experimental [8] works have considered the problem of muon transfer from the muonic hydrogen to an oxygen molecule. Since the muonic hydrogen has to approach one of the oxygen nuclei very close in order for the muon to be transferred [9], the process can be described as



Although there have been several full three-dimensional calculations of muon transfer rates at low energies between muonic-hydrogen and low- Z atoms (see literature cited in Ref. [6]), there is none when the transfer involves nuclei with $Z > 3$. Indeed, as Z increases there is a larger initial-channel polarization and a stronger final-channel Coulomb interaction which make the full quantum calculation computationally heavy. Thus up to now only approximate calculations have been performed for the muon-transfer rate between muonic-hydrogen and oxygen [4, 7, 9, 10]. We present here the first numerically converged three-dimensional calculations for reaction (1) for s waves and collision energies in the range $10^{-3} - 10^3$ eV. Since for the entrance channel the centrifugal barrier for $J = 1$ is about 0.1 eV, the calculations presented here can be considered as full 3-dimensional up to thermal energies.

The calculation were performed as follows. Hyperspherical elliptic coordinates [11, 12] have been used. A piecewise diabatic basis set on the hyperspherical angles was used to expand the wave function. The resulting close-coupling time-independent Schrödinger equations in the hyper-radius were solved using a de Vogelaere algorithm and the partial and total muon-transfer probabilities were determined by the standard S-matrix analysis at large distances. Since for energies below 10^{-1} eV, the muon-transfer process studied here is equivalent to an ultra-cold collision (de Broglie wavelength, $\lambda > 1$ Å, much larger than the effective range, $a \sim 0.1$ Å, of the potential interaction), special care had to be taken to the asymptotic analysis in the entrance channel.

The paper is organized as follows. Section II introduces the model and the methodology used in the calculations. Section III presents the calculated muon-transfer probabilities together with their interpretation in terms of simple Landau-Zener and threshold models. Finally, section IV is devoted to the conclusions.

II. METHODOLOGY

We start with the two mass-scaled Jacobi sets of coordinates $(\mathbf{R}_1, \mathbf{r}_1)$ and $(\mathbf{R}_2, \mathbf{r}_2)$ adapted to the entrance and exit channels of reaction (1), respectively (see fig. 1). They are defined by

$$\mathbf{R}_i = \sqrt{\frac{m_{i,jk}}{m}} \left(\frac{m_j \mathbf{x}_j + m_k \mathbf{x}_k}{m_j + m_k} - \mathbf{x}_i \right), \quad (2)$$

$$\mathbf{r}_i = \sqrt{\frac{m_{j,k}}{m}} (\mathbf{x}_j - \mathbf{x}_k), \quad (3)$$

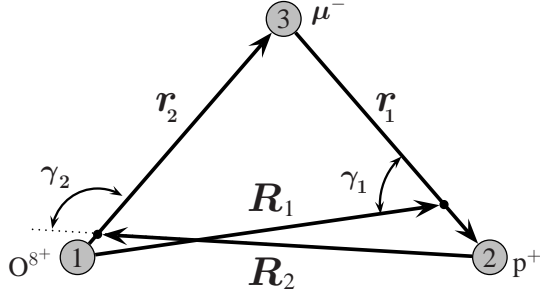


FIG. 1: The two sets of mass-scaled Jacobi coordinates corresponding to the entrance and exit channel of reaction (1). The center of mass positions are not in scale.

where the set $(i = 1, j = 2, k = 3)$ corresponds to (O, p, μ) , and $(i = 2, j = 3, k = 1)$ to (p, μ, O) . The reduced masses $m_{i,jk}$ and $m_{j,k}$ in Eqs. (2) and (3), are given by

$$m_{i,jk} = \frac{m_i(m_j + m_k)}{m_i + m_j + m_k}, \quad m_{j,k} = \frac{m_j m_k}{m_j + m_k}, \quad (4)$$

while m is chosen as

$$m = \left(\frac{m_i m_j m_k}{m_i + m_j + m_k} \right)^{1/2}. \quad (5)$$

These sets are related by the orthogonal transformation

$$\begin{pmatrix} \mathbf{R}_2 \\ \mathbf{r}_2 \end{pmatrix} = \begin{pmatrix} -\cos\theta_\mu & -\sin\theta_\mu \\ \sin\theta_\mu & -\cos\theta_\mu \end{pmatrix} \begin{pmatrix} \mathbf{R}_1 \\ \mathbf{r}_1 \end{pmatrix}, \quad (6)$$

where

$$\tan\theta_\mu = \frac{m_\mu}{m}, \quad (7)$$

giving in our case $\theta_\mu \simeq 19^\circ$.

In spherical coordinates, the system can be described by three Euler angles specifying the overall orientation, the two distances (R_i, r_i) and the angle γ_i between the two vectors \mathbf{R}_i and \mathbf{r}_i (see figure 1). Two sets of Delves hyperspherical coordinates are then defined by the common hyper-radius

$$\rho = \sqrt{R_i^2 + r_i^2} \quad (8)$$

the hyper-angles

$$\tan(\chi_i/2) = \frac{r_i}{R_i}; \quad i = 1, 2. \quad (9)$$

and the γ_i angles.

The relationship between the two sets of Delves shape angles is given by

$$\begin{aligned} & \begin{pmatrix} \cos\chi_2 \\ \sin\chi_2 \cos\gamma_2 \\ \sin\chi_2 \sin\gamma_2 \end{pmatrix} \\ &= \begin{pmatrix} \cos(2\theta_\mu) & \sin(2\theta_\mu) & 0 \\ -\sin(2\theta_\mu) & \cos(2\theta_\mu) & 0 \\ 0 & 0 & 1 \end{pmatrix} \begin{pmatrix} \cos\chi_1 \\ \sin\chi_1 \cos\gamma_1 \\ \sin\chi_1 \sin\gamma_1 \end{pmatrix} \quad (10) \end{aligned}$$

The hyperspherical elliptic coordinates are defined by

$$\eta = \chi_1 - \chi_2, \quad -2\theta_\mu \leq \eta \leq 2\theta_\mu, \quad (11a)$$

$$\xi = \chi_1 + \chi_2, \quad 2\theta_\mu \leq \xi \leq 2\pi - 2\theta_\mu, \quad (11b)$$

with the volume element

$$d\tau = \rho^5 d\rho \frac{\pi^2}{4 \sin(2\theta_\mu)} (\cos(\eta) - \cos(\xi)) d\eta d\xi. \quad (12)$$

In terms of these coordinates the kinetic energy operator for total angular momentum zero, is given by

$$T = -\frac{\hbar^2}{2m} \left(\frac{1}{\rho^5} \frac{\partial}{\partial \rho} \rho^5 \frac{\partial}{\partial \rho} + \frac{16}{\rho^2} \frac{1}{\cos(\eta) - \cos(\xi)} \left[\frac{\partial}{\partial \eta} \left(\cos(\eta) - \cos(2\theta_\mu) \right) \frac{\partial}{\partial \eta} - \frac{\partial}{\partial \xi} \left(\cos(\xi) - \cos(2\theta_\mu) \right) \frac{\partial}{\partial \xi} \right] \right), \quad (13)$$

For a given value of the hyper-radius ρ , the total wave function $\psi(\rho, \eta, \xi)$ is expanded in terms of a basis set of N_{ch} functions $\phi_i(\eta, \xi; \rho)$ depending on the hyperspherical angles η and ξ . We use a diabatic-by-sector representation. In each sector $\rho_n - \delta\rho_n \leq \rho < \rho_n + \delta\rho_n; n = 1, \dots, N_\rho$ we write:

$$\psi(\rho, \eta, \xi) = \frac{1}{\rho^{5/2}} \sum_{i=1}^{N_{ch}} F_i(\rho) \phi_i(\eta, \xi; \rho_n) \quad (14)$$

where $\phi_i(\eta, \xi; \rho_n)$ are eigenstates of the Hamiltonian at fixed ρ_n distances. Their calculation requires the solution of a bound state problem for the Coulomb potential

$$V = -\frac{e^2}{|\mathbf{x}_p - \mathbf{x}_\mu|} - \frac{8e^2}{|\mathbf{x}_\mu - \mathbf{x}_O|} + \frac{8e^2}{|\mathbf{x}_p - \mathbf{x}_O|} \quad (15)$$

presenting two attractive singularities at $(\eta, \xi) = (\pm 2\theta_\mu, 2\theta_\mu)$ corresponding to a vanishing muon-oxygen and muon-proton distance.

This bound state problem can be rewritten as:

$$\left\{ -\frac{16\hbar^2}{2m\rho_n^2} [\hat{L}(\eta) - \hat{L}(\xi)] + W(\rho_n, \eta, \xi) \right\} \phi_i(\eta, \xi; \rho_n) = 0, \quad (16)$$

where

$$\hat{L}(u) = \frac{\partial}{\partial u} (\cos u - \cos(2\theta_\mu)) \frac{\partial}{\partial u} \quad (17)$$

and

$$W(\rho_n, \eta, \xi) = [\cos(\eta) - \cos(\xi)] [V(\rho_n, \eta, \xi) - \epsilon_i(\rho_n)]. \quad (18)$$

Equation (16) can be viewed as a zero eigenvalue problem depending parametrically on the potential $[\cos(\eta) - \cos(\xi)] [V(\rho_n, \eta, \xi) - \epsilon_i(\rho_n)]$, in the sense that the constant

$\epsilon_i(\rho_n)$ is being adjusted in such a way that the operator on the left hand side of equation (16) has zero eigenvalue. The renormalized potential $W(\rho_n, \eta, \xi)$ has two important features. One is that the two Coulomb singularities are regularized, the other being that it is approximately separable. We can therefore write

$$W(\rho_n, \eta, \xi) = W_\eta(\rho_n, \eta) + W_\xi(\rho_n, \xi) + \Delta W(\rho_n, \eta, \xi), \quad (19)$$

where $W_\eta(\rho_n, \eta) = W(\rho_n, \eta, 2\theta_\mu)$ and $W_\xi(\rho_n, \xi) = W(\rho_n, -2\theta_\mu, \xi) - W(\rho_n, -2\theta_\mu, 2\theta_\mu)$.

The 2-dimensional problem can be solved by exploiting this approximate separability of the potential. For instance, defining $\eta = 2\theta_\mu \bar{\eta}$ with $-1 \leq \bar{\eta} \leq 1$, we get from equation (16)

$$\left[-\frac{4\hbar^2}{m\rho_n^2} \frac{s^2(\theta_\mu)}{\theta_\mu^2} \frac{\partial}{\partial \bar{\eta}} \left(1 - \frac{\sin^2 \theta_\mu \bar{\eta}}{\sin^2 \theta_\mu} \right) \frac{\partial}{\partial \bar{\eta}} + W_\eta(\rho_n, \eta) \right] \varphi_k(\eta; \rho_n) = \epsilon_k^{(\eta)}(\rho_n) \varphi_k(\eta; \rho_n) \quad (20)$$

The similarity between the differential operator in (20) (in particular in the limit $\theta_\mu \rightarrow 0$) with the one defining Legendre polynomials, suggests to use the latter as basis set functions for expansion of $\varphi_k(\eta; \rho_n)$. We solve a similar problem for ξ using the $W_\xi(\rho_n, \xi)$ potential and obtain $\varphi_\ell(\xi; \rho_n)$ eigenfunctions and the $\epsilon_\ell^{(\xi)}(\rho_n)$ eigenvalues. We then iterate (using a bi-section method on ϵ_i) until we get $\epsilon_k^{(\eta)}(\rho_n) + \epsilon_\ell^{(\xi)}(\rho_n) = 0$. Once the separable basis set is obtained, solutions of (16) for the full non-separable potential are obtained by diagonalizing the representation matrix of the full Hamiltonian in the product basis. In Fig. 2 we present the calculated energies ϵ_i as a function of the hyper-radius ρ . The origin of energies has been chosen to coincide with the asymptotic limit of the entrance channel $(p\mu)_{n=1} + O$. The calculations presented in this work cover the energy range between this limit and the $p + (\mu O)_{n=10}$ threshold at about 1 keV.

The N_{ch} coupled equations are integrated along the hyper-radius ρ using the de Vogelaere algorithm [13]. This provides a logarithmic derivative matrix Z at $\rho_M = \rho_{N_\rho} + \delta_{N_\rho}$. For the energy range considered here, we included 88 channels: $((p\mu)_{n=1-2} + O$ and $p + (\mu O)_{n=1-9}$. The integration of the coupled equations was performed from the origin to $\rho_{\text{end}} \sim 200 a_\mu \sim 1 \text{ \AA}$. The asymptotic analysis has been performed using the appropriate Jacobi coordinates for the entrance and for the product channels. Elementary asymptotic wave functions for the different final arrangement channels $\lambda = 1, 2$ are written as products of translational functions $f_{n\ell}(R_\lambda)$, Coulomb bound wave functions $C_{n\ell}(r_\lambda)$ and normalized Legendre polynomials:

$$\psi_{n\ell\lambda}(R_\lambda, r_\lambda, \gamma_\lambda) = f_{n\ell}(R_\lambda) C_{n\ell}(r_\lambda) \bar{P}_\ell(\cos \gamma_\lambda). \quad (21)$$

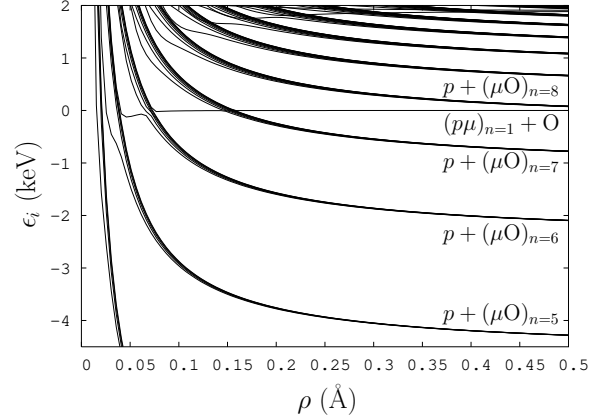


FIG. 2: Calculated ϵ_i energies of the hyperspherical elliptic basis as a function of the hyper-radius.

We use these elementary asymptotic wave functions to form N_{ch} physical solutions whose forms are given by

$$\Psi^{(a)} = \psi_{n\ell\lambda}^S(R_\lambda, r_\lambda, \gamma_\lambda) + \sum_{n'\ell'\lambda'} \psi_{n'\ell'\lambda'}^C(R_{\lambda'}, r_{\lambda'}, \gamma_{\lambda'}) K_{n'\ell'\lambda' \leftarrow n\ell\lambda} \quad (22)$$

where the superscripts S and C refer to the type of translational functions (S for sine-type functions for open channels and exponentially decaying functions for closed channels, C for cosine-type and exponentially growing functions, respectively). If a Coulombic interaction is still important (as for instance in the product channels $O\mu + p$ in our problem), Coulomb wave functions are used

instead.

We define the matrices \mathbf{F} and \mathbf{F}' as the projections of the elementary asymptotic functions on the ϕ_i hyper-

spherical basis. This projection is performed at the maximum hyperspherical radius ρ_M

$$F_{i,n\ell\lambda} = \langle \phi_i | \psi_{n\ell\lambda} \rangle_{\rho=\rho_M} = \int d\eta d\xi [\cos(\eta) - \cos(\xi)] \phi_i(\eta, \xi; \rho_M) \psi_{n\ell\lambda}(R_\lambda, r_\lambda, \gamma_\lambda)|_{\rho_M} \quad (23a)$$

$$F'_{i,n\ell\lambda} = \langle \phi_i | \partial \psi_{n\ell\lambda} / \partial \rho \rangle_{\rho=\rho_M} = \int d\eta d\xi [\cos(\eta) - \cos(\xi)] \phi_i(\eta, \xi; \rho_M) \partial \psi_{n\ell\lambda}(R_\lambda, r_\lambda, \gamma_\lambda) / \partial \rho|_{\rho_M} \quad (23b)$$

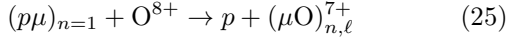
The N_{ch} linearly independent solutions which result from the propagation steps up to ρ_M are linear combinations of the N_{ch} asymptotic solutions given by equations (23). This can be restated as an equality of the logarithmic derivative matrix \mathbf{Z} in the hyperspherical basis

$$\mathbf{Z} = (\mathbf{F}'^S + \mathbf{F}'^C \mathbf{K})(\mathbf{F}^S + \mathbf{F}^C \mathbf{K})^{-1} \quad (24)$$

The \mathbf{K} matrix, and then the \mathbf{S} matrix, can be extracted from (24).

III. RESULTS OF THE CALCULATIONS

We have performed calculations of the reaction



for collision energies in the range $10^{-3} - 10^3$ eV and for total angular momentum $J = 0$ (s waves). For large R distance between the oxygen nuclei and the proton, the potential for the entrance channel of reaction (25) behaves as $V = -\alpha Z^2 e^2 / 2R^4$, where $Z = 8$ and $\alpha = (9/2)(\hbar^2 / m_{\mu,p} e^2)^3$. Since with this potential the centrifugal barrier has a height of $(\hbar^2 J(J+1) / m_{O,p\mu} Z e)^2 / 8\alpha$, for energies below 0.1 eV the partial wave $J = 0$ is the only one which contributes to the cross sections. Thus for thermal energies these calculations are essentially exact full 3-dimensional.

Fig. 3 presents the total probabilities for muon transfer as a function of the energy, as well as the partial muon-transfer probabilities into the $p + (\mu O)_{n=6}$ and $p + (\mu O)_{n=5}$ channels. The other open channels have negligible populations. This is in complete agreement with what was found in approximate calculations [9]. These results can be qualitatively understood by inspection of figure 2. Starting in channel $(p\mu)_{n=1} + O$, the system crosses diabatically the channel $p + (\mu O)_{n=7}$. Muon transfer is completely negligible as the coupling is very small compared with the collision energy. The couplings to channels $p + (\mu O)_{n=6}$ and $p + (\mu O)_{n=5}$ are larger as evidenced by avoided crossings. The other channels $p + (\mu O)_{n<5}$ are weakly coupled to the initial one and they are not expected to be populated significantly.

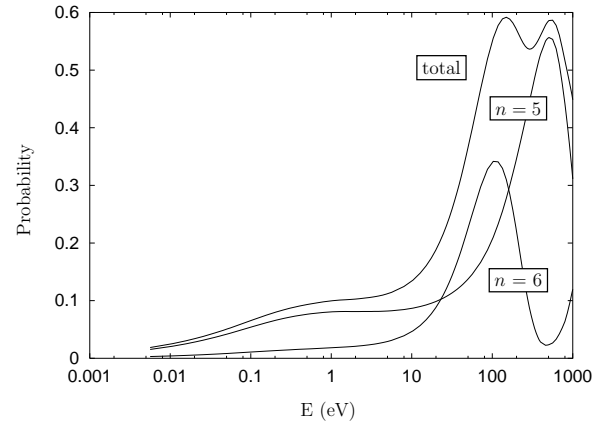


FIG. 3: Partial and total muon-transfer probabilities for reaction (25) as a function of the collision energy.

Actually, a simple calculation involving only three channels $((p\mu)_{n=1} + O, p + (\mu O)_{n=5-6, \ell=0})$ and using the semi-classical Landau-Zener formula for the two crossings provides qualitative agreement with the exact results down to energies of the order of 1 eV (see figure 4). For lower energies, quantum threshold behavior dominates the semi-classical Landau-Zener approximation and for very low energies Wigner's threshold laws predict a $E^{1/2}$ dependence. This low energy region corresponds to $k a \ll 1$, with $k = (2m_{O,p\mu} E)^{1/2} / \hbar$ and a being the range of the potential in the entrance channel. Defining the effective range of the potential by $V(a) \leq E$, we get $E \ll 0.1$ eV. This is exactly what it is found in our calculations (see figure 3).

In figures 5 and 6 we present relative populations of $O\mu_{n=5-6, \ell}$ levels for collision energy $E = 0.1$ eV. This distribution is almost independent of collision energy in the energy range considered here. This fact and the particular form of the distributions in figures 5 and 6 can be understood as follows. From an inspection of figure 2 it is clear that only one of the set of states correlating asymptotically to a given $O\mu_n$ manifold is significantly coupled to the initial $p\mu_{n=1}$ state. Due to the approximate separability of the potential, each of these states can be assigned to approximate hyperspherical elliptic

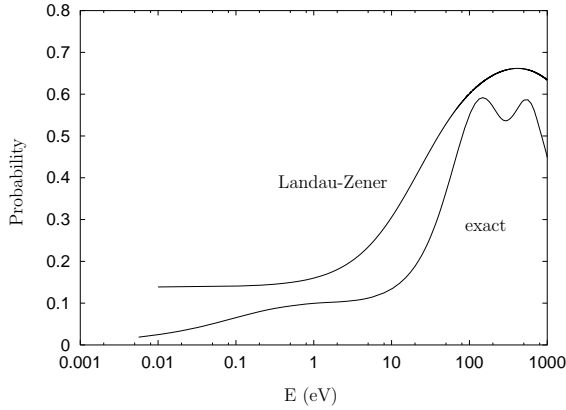


FIG. 4: Total muon-transfer probabilities for reaction (25) as a function of the collision energy using a simple three channel problem and Landau-Zener semi-classical approximation.

quantum numbers (n_η, n_ξ) . Since the initial $p\mu_{n=1}$ channel is colinearly dominated and $n_\xi > 0$ corresponds to excitation away from the colinear configuration, the final states significantly coupled to the initial channel satisfy the approximate selection rule: $n_\xi = 0$. At large distances, hyperspherical coordinates tend gradually toward parabolic coordinates[12]. The final $(n_\eta, n_\xi = 0)$ states can therefore be identified to $(\bar{n}_\eta, \bar{n}_\xi = 0)$ states with $\bar{n}_\eta = n - 1$ and $\bar{n}_\xi = n_\xi$. The final approximate ℓ distribution is then given by the square of the projection of this states onto the final (n, ℓ) spherical basis set with the result [14]:

$$P_{n\ell}^{app} \propto |C((n-1)/2, (n-1)/2, -n/2, -n/2; \ell, 0)|^2 \quad (26)$$

where C stands for a Clebsh-Gordan coefficient. We have represented this approximate distribution in figures 5 and 6. Clearly, the $n_\xi = 0$ selection rule is a very good approximation.

Experimentally only the populations of the fine-structure levels j are eventually measurable. Thus, from the orbital angular momentum ℓ probabilities one gets

$$P_{n,j} \propto \sum_{\ell} \frac{P_{n,\ell}}{2\ell+1} \sum_{m_j, m_\ell} |C(\ell, 1/2, m_\ell, m_j - m_\ell; j, m_j)|^2 \quad (27)$$

The results are presented in figure 7.

IV. CONCLUSIONS

We have presented 3-dimensional calculations of muon transfer probabilities between muonic hydrogen and oxygen for relative translational energies between 10^{-3} and 10^3 eV and total angular momentum $J = 0$ (s waves). Since the centrifugal barrier for $J = 1$ is of the order of 0.1 eV, for thermal and lower energies the calculations are essentially exact.

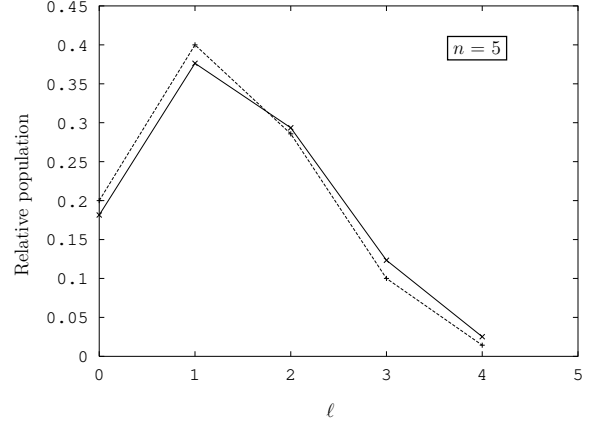


FIG. 5: Exact (full line) and approximate (dotted) relative populations of the ℓ levels for $n = 5$ and collision energy $E = 0.1$ eV.

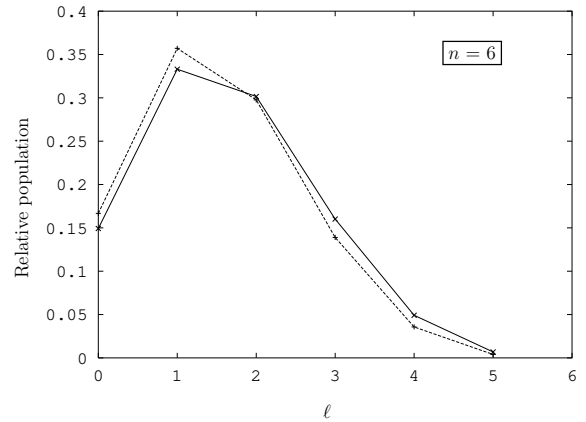


FIG. 6: Exact (full line) and approximate (dotted) relative populations of the ℓ levels for $n = 6$ and collision energy $E = 0.1$ eV.

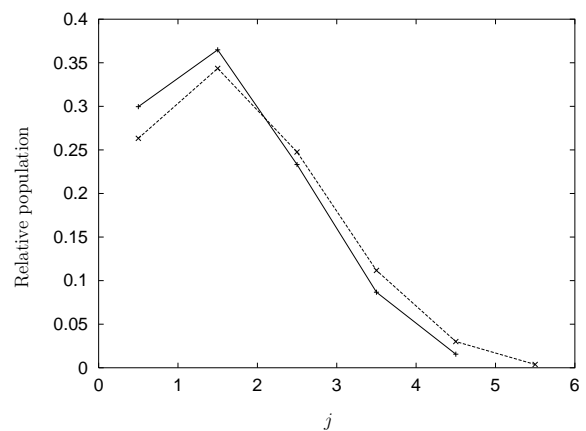


FIG. 7: Relative populations of the j levels for $n = 5$ (dotted) and $n = 6$ (full) for a collision energy $E = 0.1$ eV.

The results for the total and partial probabilities can be interpreted qualitatively by a simple three channels model and Landau-Zener semi-classical approximation for energies between 1 and 1000 eV. For energies below 0.1 eV, the probabilities follow the expected Wigner's threshold laws behavior.

The fine-structure levels populations are essentially independent of energy and almost independent of the principal quantum number n . This has been attributed to an approximate selection rule for the elliptic hyperspherical quantum number n_ξ .

In conclusion, the hyperspherical elliptic coordinates

introduced by Tolstikhin *et al* [11], are particularly well suited to the treatment of this type of reaction.

Acknowledgments

We thank IDRIS (CNRS computing center) for an allocation of CPU time on a NEC SX5 vector processor, and NATO for a collaborative linkage grant PST.CLG.978454 between Bulgaria and France.

- [1] L. I. Ponomarev, *Hyperfine Interact.* **138**, 15 (2001).
- [2] D. Bakalov, E. Milotti, C. Rizzo, A. Vacchi, and E. Zavattini, *Phys. Lett. A* **172**, 277 (1993).
- [3] A. Dupays, B. Lepetit, J. A. Beswick, C. Rizzo, and D. Bakalov, *Phys. Rev A*, in press (2003).
- [4] R. A. Sultanov and S. K. Adhikari, *Phys. Rev. A* **62**, 22509 (2000).
- [5] A. Adamczak, D. Bakalov, K. Bakalova, E. Polacco, and C. Rizzo, *Hyperfine Interact.* **136**, 1 (2001).
- [6] R. A. Sultanov and S. K. Adhikari, *J. Phys. B: At. Mol. Opt. Phys.* **35**, 935 (2002).
- [7] A. Dupays, B. Lepetit, J. A. Beswick, C. Rizzo, and D. Bakalov, *Phys. Rev A* **67**, 062505 (2003).
- [8] A. Werthmüller, A. Adamczak, R. Jacot-Guillarmod, L. S. F. Mulhauser, L. Schellenger, H. Schneuwly, Y. Thalmann, and S. Tresch, *Hyperfine Interact.* **116**, 1 (1998).
- [9] S. S. Gershtein, *Zh. Eksp. Teor. Fiz.* **43**, 706 (1962), *sov. Phys. JETP* **16**, 501 (1963).
- [10] P. K. Haff, E. Rodrigo, and T. A. Tombrello, *Ann. Physics* **104**, 363 (1977).
- [11] O. I. Tolstikhin, S. Watanabe, and M. Matsuzawa, *Phys. Rev. Lett.* **74**, 3573 (1995).
- [12] O. I. Tolstikhin and M. Matsuzawa, *Phys. Rev. A* **63**, 62705 (2001).
- [13] B. Lepetit, J. M. Launay, and M. L. Dourneuf, *Chem. Phys.* **106**, 103 (1986).
- [14] D. Park, *Z. Phys.* **159** (1960).